catalysts

Supporting Information: Spray-dried Ni Catalysts with Tailored Properties for CO_2 Methanation

Bjarne Kreitz [1,*,†], Aurina Martínez Arias [2,†], Jan Martin [1], Alfred P. Weber [2] and Thomas Turek [1]

[1] Institute of Chemical and Electrochemical Process Engineering, Clausthal University of Technology, Leibnizstr. 17, 38678 Clausthal-Zellerfeld, Germany; martin@icvt.tu-clausthal.de (J.M.); turek@icvt.tu-clausthal.de (T.T.)

[2] Institute of Particle Technology, Clausthal University of Technology, Leibnizstr. 19, 38678 Clausthal-Zellerfeld, Germany; aurina.martinez.arias@tu-clausthal.de (A.M.A.); weber@mvt.tu-clausthal.de (A.P. W.)

* Correspondence: kreitz@icvt.tu-clausthal.de; Tel.: +49-5323-72-2473

† These authors contributed equally to this work.

1. Sintering of Silica Particles

High calcination temperatures lead to the sintering of the silica support and the Ni crystals. The effect of sintering for the silica support is illustrated in Figure S1. Figure S1a shows the BET surface and total pore volume for the pure SiO_2 support. Pure SiO_2 particles with BB(20) were produced with the same spray-drying procedure only without the Ni nitrate. BET surface area and pore volume remain constant up to a calcination temperature of 800 K, but then a significant sintering sets in. The particles are completely sintered after heat treatment at 1200 K for 4 h. Figure S1b shows the SEM micrograph after calcination at 673 K that reveals spherical SiO_2 particles. In contrast, Figure S1c displays the SiO_2 particles after heat treatment at 1273 K, which proves the sintering. Within this study, calcination temperatures for the catalysts of 973 K were applied. Adding Ni to the silica hinders the SiO_2 particles from sintering, which is seen by the BET measurements provided in Table 1 in the main manuscript.

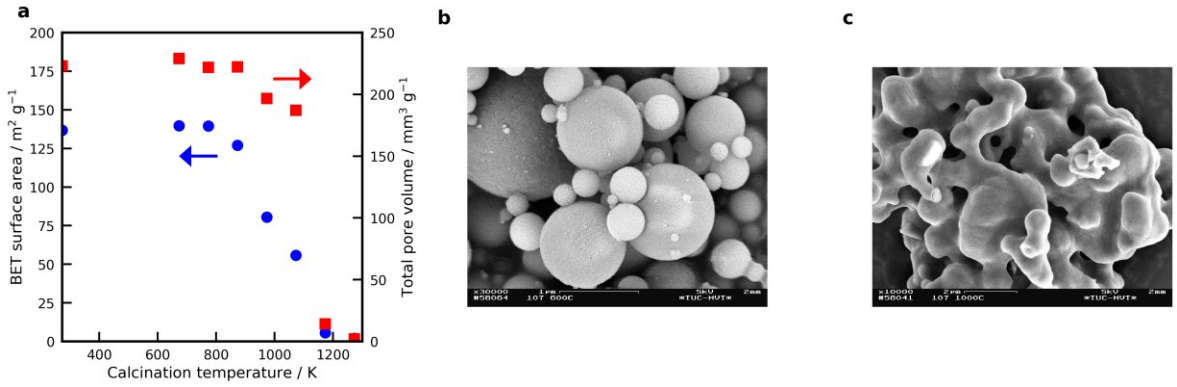


Figure S1. (a) BET surface area and pore volume of SiO_2 with BB(20) at different calcination temperatures. **(b)** SEM image for the calcination at 673 K. **(c)** SEM image after calcination at 1273 K.

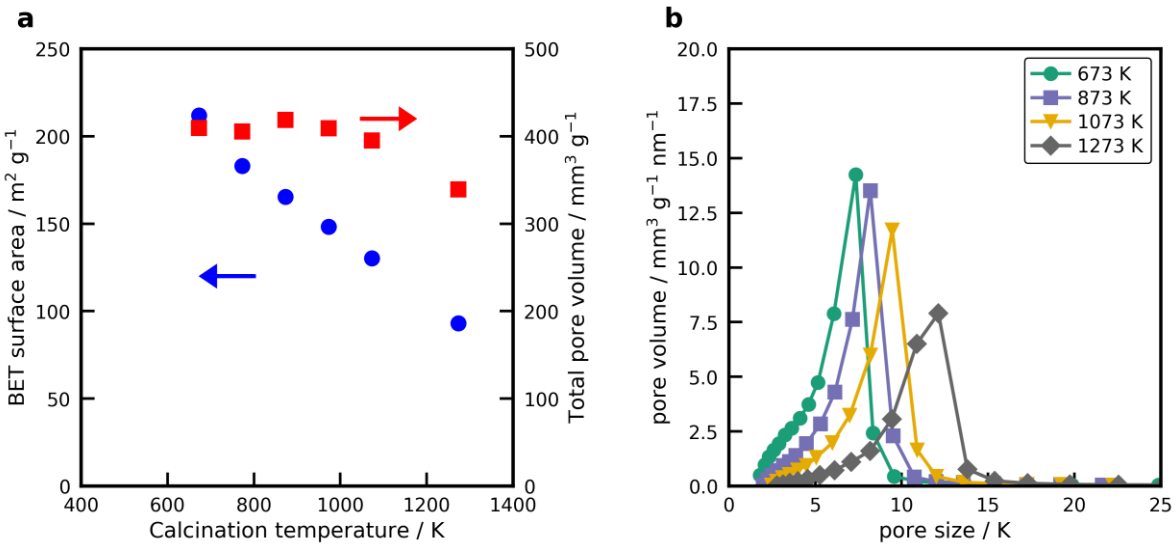


Figure S2. (a) BET surface area and pore volume of the Al_2O_3at different calcination temperatures. **(b)** Pore size distribution for different calcination temperatures.

2. TEM Images

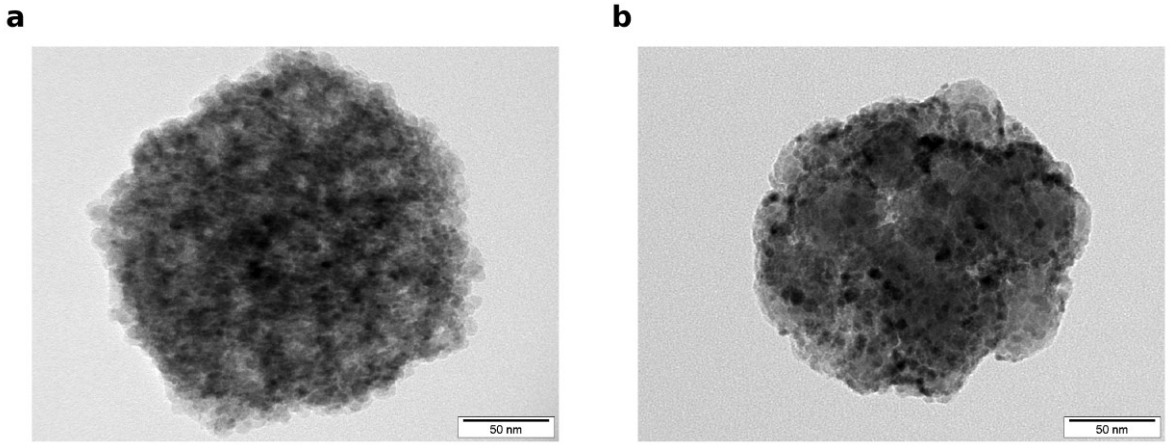


Figure S3. TEM micrograph of Ni/SiO_2 catalyst with **(a)** BB(8) with 20 wt% calcined at 673 K and **(b)** BB(45) with 5 wt% calcined at 673 K.

3. TGA

Table S1 summarizes the thermogravimetric analysis of the catalysts, which were not further heat-treated after the production. These samples show an incomplete decomposition of the nitrates, that is why they loose mass during the reduction. The percentage mass loss at the reduction temperature was required to determine the actual mass of the catalyst sample.

Table S1. The thermogravimetric analysis of the catalysts, which were not further heat-treated after the production. These samples show an incomplete decomposition of the nitrates.

	unit	1a	2a	3a	4a	5a	6a
mass loss	%	19.3	11.2	14.3	14.4	21.6	21.9

4. XRD

Figure S4a shows the recorded XRD patterns for the spray-dried Ni/Al_2O_3 catalyst after production and after calcination at 673 K. Directly after production a boehmite structure is obtained. This transforms after calcination to the γ-Al_2O_3 phase. However, in both cases no crystalline NiO is observed, which indicates that the NiO reacts with the Al_2O_3 and forms crystalline $NiAl_2O_4$. Figure S4c compares the lattice constant of γ-Al_2O_3 in dependence of the Ni loading with results from Zhou et al. [1] and O'Neil et al. [2].

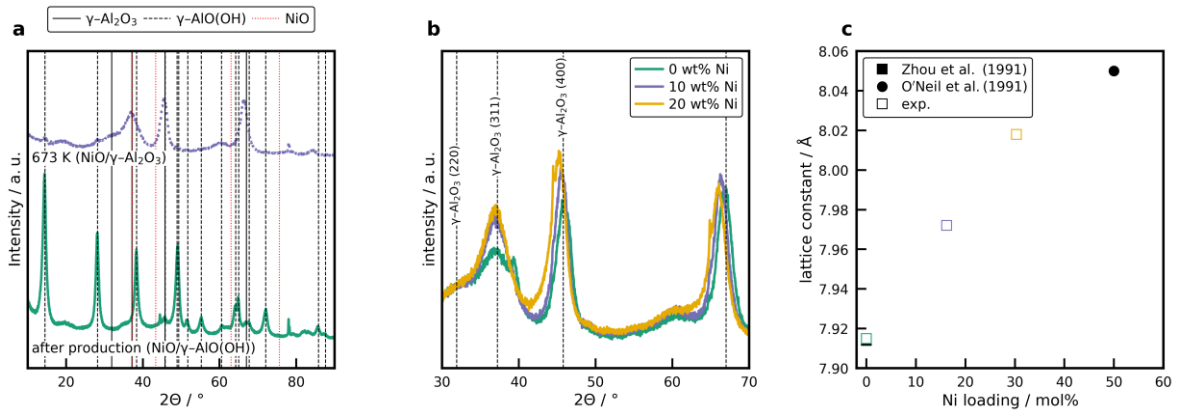


Figure S4. (a) XRD patterns of the spray-dried Ni/Al_2O_3 catalyst after production and after calcination at 673 K. Reflections for γ-Al_2O_3, γ-AlO(OH), and NiO are marked. **(b)** XRD patterns of BB(Al_2O_3) calcined at 673 K with different nickel loadings. **(c)** Lattice constant of the crystalline structure as a function of the Ni loading in BB(Al_2O_3).

Table S2. Average NiO particle sizes (in nm) determined with XRD for the Ni/SiO_2 catalysts with different Ni loadings and SiO_2 primary particle sizes of 8 nm, 20 nm and 45 nm after calcination at different temperatures. The last row is the m_{Ni}/a_{SiO_2} ratio.

Temperature / K	BB(20)			BB(8)		BB(45)
	20 wt%	10 wt%	5 wt%	20 wt%	10 wt%	7 wt%
273	4.5	3.2	2.1	4.3	2.0	-
473	5.2	4.0	2.7	4.4	2.1	3.51
573	5.7	4.3	2.7	4.5	2.3	3.57
673	6.8	4.7	2.8	5.1	2.5	3.97
773	7.2	4.9	2.9	5.3	2.5	4.11
873	7.7	4.9	3.3	5.4	2.6	4.65
973	8.3	5.4	3.3	5.9	2.8	4.59
m_{Ni}/a_{SiO_2}/mg m^{-2}	2.0	1.13	0.40[†]	1.23	0.56	1.19[†]

[†]No measured Ni loadings from ICP are available for these samples and the m_{Ni}/a_{SiO_2} is calculated with the nominal loading. This value is subjected to a higher error.

5. SAXS

The result from the SAXS measurement is displayed in Figure S6 for the Ni/SiO_2 catalyst with BB(20) 20 wt% calcined at 673 K. Several peaks are observed for different particle sizes. The first peak at 7.0 nm corresponds to the Ni crystals. This agrees well with the XRD result of 6.8 nm. The peak with the maximum at 27 nm can be associated with the primary SiO_2 particles, which have a nominal particle size of 20 nm. Remaining peaks at higher diameters of 50 and 95 nm can either be an error from the fitting procedure of the SAXS evaluation due to a high signal-to-noise ratio or small Ni/SiO_2 agglomerates.

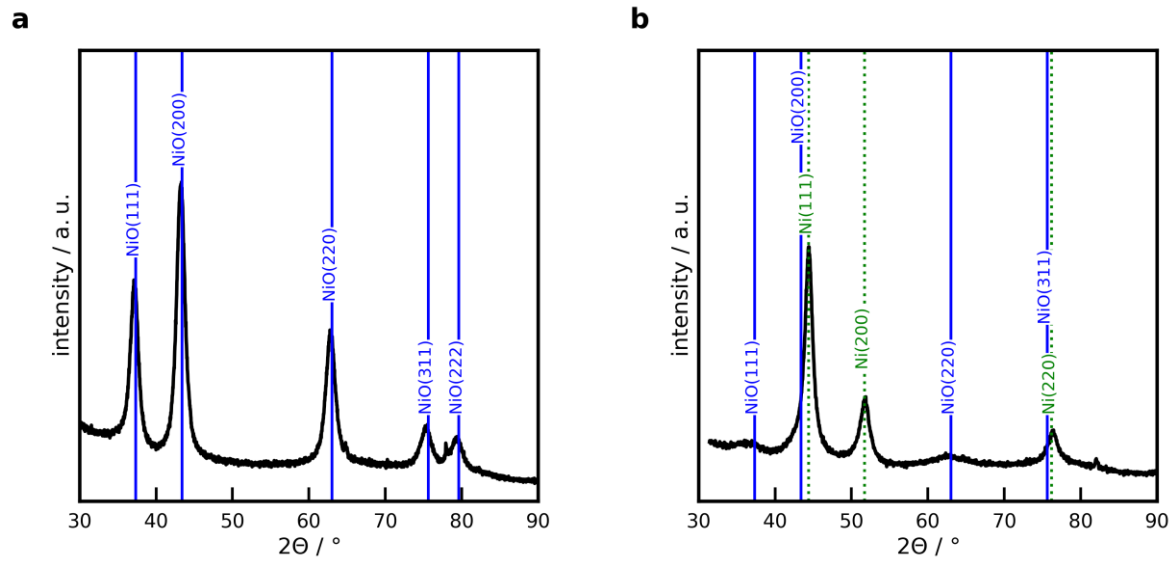


Figure S5. (a) XRD patterns for the BB(20) catalyst with 20 wt% calcined at 673 K. **(b)** XRD pattern for the same catalyst after reduction and passivation.

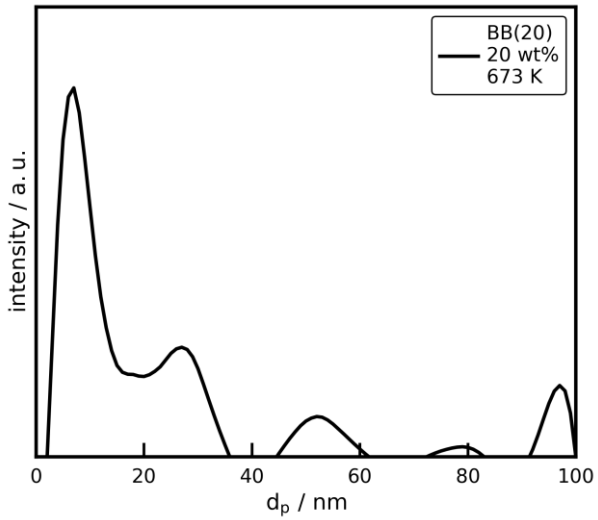


Figure S6. SAXS measurement of BB(20) with 20 wt% calcined at 673 K.

6. Chemisorption

Recorded adsorption isotherms are provided in Figure S7. Figure S7a shows the adsorption isotherms for the BB(8) and 20 wt% catalyst for different calcination temperatures. With increasing calcination temperature, the adsorbed amount of H_2 decreases because the Ni crystal sinter and the DOR is lower. Double CO_2 adsorption isotherms are shown in Figure S7b for BB(8), 20 wt%, without heat treatment. Between the isotherms, the sample is evacuated for 1 h at adsorption temperature. The catalyst shows a high initial CO_2 uptake at low pressures, followed by a linear increase. The initial uptake is a result of adsorption on the Ni crystal. As shown by the measurement of the pure support, the SiO_2 surface does not provide basic surface sites. The second isotherm further proves this for the catalyst, which shows only a CO_2 uptake at high pressures indicating basic sites with a weak binding strength on the support.

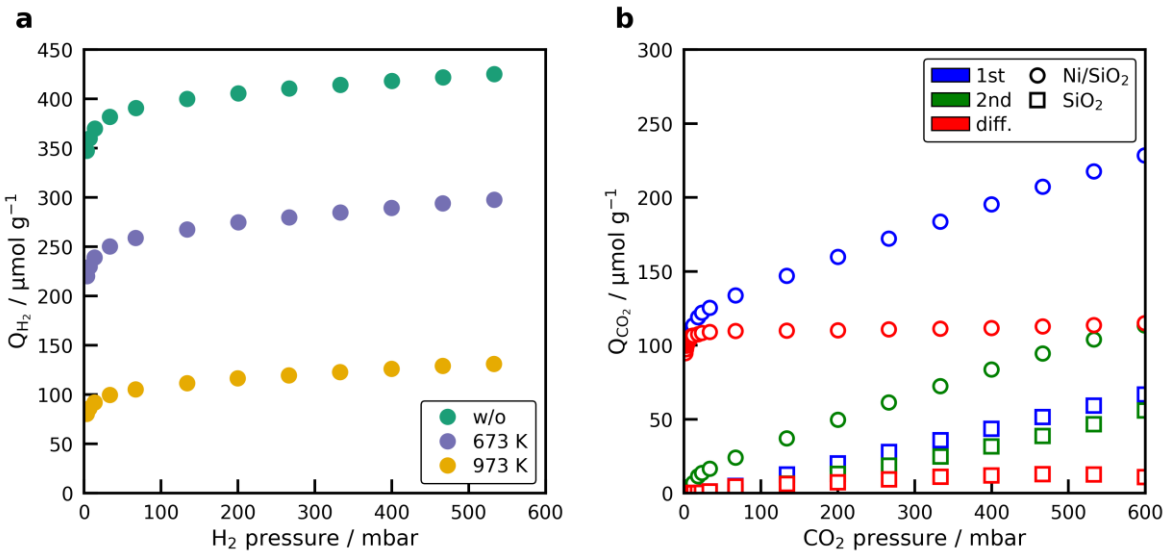


Figure S7. (a) Volumetric adsorption isotherms for H_2 adsorption on BB(8), 20 wt% at different calcination temperatures **(b)** CO_2 adsorption isotherm for the Ni/SiO_2 catalyst with BB(8), 20 wt%, without calcination and the pure SiO_2 support.

7. Temperature-programmed reduction

Figure S8 shows the recorded ion currents during the TPR of the BB(8) catalyst with 10 wt% Ni and without heat treatment. At low temperatures a desorption of CO_2 and at higher temperatures CO (CO^+) is observed. The catalyst is exposed to air and adsorbs CO_2, which is not entirely removed during the degassing. Due to the adsorbed CO_2, a small methane formation (CH_3^+) is recorded. The decomposition peak of the nitrates and the release of NO and NO_2 (NO^+) has the same position and shape as the recorded TCD signal. It cannot be differentiated between NO and NO_2, since both components form a fragment on the *m*/*z*-ratio of 30.

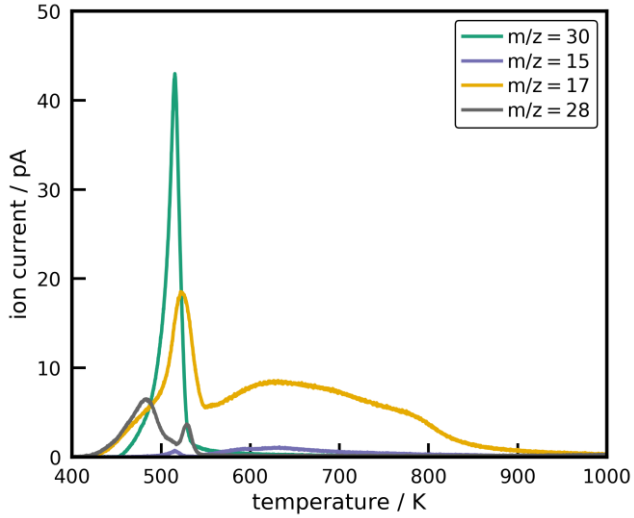


Figure S8. TPR profile of the Ni/SiO_2 (BB(8), 10 wt%, without calcination) recorded with the MS. Mass-to-charge (*m*/*z*) ratios of 30 (NO^+), 15 (CH_3^+), 17 (OH^+), and 28 (CO^+) are displayed.

8. Activation energies

Figure S9 shows the Arrhenius diagram for some selected samples. The activation energies determined for the catalysts are in a narrow range.

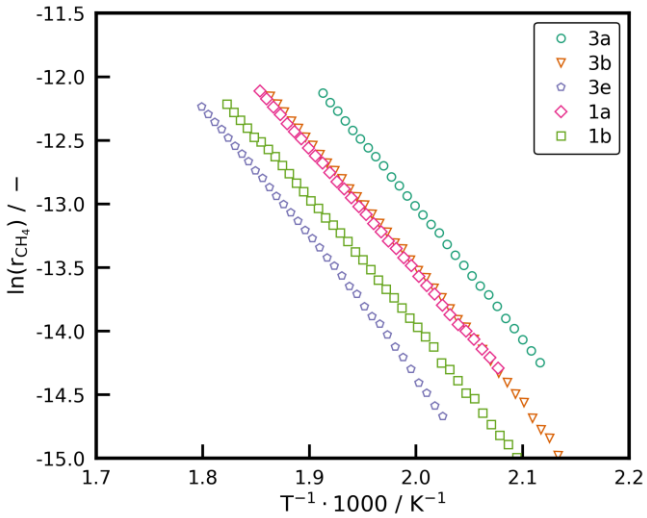


Figure S9. Arrhenius diagram for selected Ni/SiO_2 catalysts. The reaction rate was calculated with the differential fixed-bed assumption for conversions smaller than 10%. *Conditions:* m_{cat} = 30 mg, β = 20 K min^{-1}, $V_{H_2/CO_2/Ar}$ = 50 mL_N min^{-1}.

References

1. Zhou, R.-S., Snyder, R.L. Structures and transformation mechanisms of the η, γ and θ transition aluminas. *Acta Cryst.*, **1991**, *47(5)*, 617–630 doi:10.1107/S0108768191002719.
2. O'Neill, H. St. C.; Dollase, W.A.; Ross, C.R. Temperature dependence of the cation distribution in nickel aluminate (NiAl2O4) spinel: A powder XRD study. *Phys. Chem. Miner.* **1991**, *18(5)*, 302–319, doi:10.1007/BF00200188.